Applied Physics A (2023) 129:771
https://doi.org/10.1007/s00339-023-07064-4

Applied Physics A
Materials Science & Processing

Microstructure and magnetic properties of NdFe/MgO(001) thin films elaborated by evaporation from Nd_3Fe_{29} nanocrystalline powder

R. Fersi[1,2] · **A. P. Dalia**[1,3]

Received: 10 August 2023 / Accepted: 9 October 2023 / Published online: 17 October 2023

Abstract

Rare earth (R) and transition metal (T) based films are potential magnetic materials for a variety of applications. However, their structural and magnetic behavior is sensitive to growth and processing parameters. This article presents a comprehensive investigation aiming to analyze the microstructure and magnetic properties of NdFe/MgO(001) films. These films were fabricated by evaporating nanocrystalline Nd3Fe29 powder at different thicknesses (t) and subjected to various heat treatments (Ta). The main objective of this research is to gain a detailed understanding of how the structural and magnetic behavior evolves based on these parameters, which had not been achieved previously. X-ray diffraction analysis was employed to determine the crystalline structure of NdFe/MgO(001) films and to track the grain size evolution with film thickness. Scanning electron microscopy (SEM) and magnetic force microscopy (MFM) images were used to directly visualize magnetic domains and the arrangement of magnetic grains at different thicknesses. Ferromagnetic resonance (FMR) measurements revealed significant variations in resonance fields and easy axes depending on film thickness and heat treatments. The study also examined how magnetic properties such as saturation magnetization (Ms) and coercivity (Hc) are closely related to grain size, magnetic domain organization, and heat treatments. Our research produced remarkable results, especially concerning a 250 nm thick NdFe/MgO(001) film annealed at 873 K, which exhibited outstanding properties. These properties include a robust coercivity of 5230 Oe, a substantial remanent magnetization of 211 emu/cm^3, a magnetic anisotropy field of 10,325 Oe, a saturation magnetization (Ms) of 396 emu/cm^3, and a Curie temperature of approximately 388 K. It's noteworthy that this film possesses an easy magnetization axis parallel to the film plane (HFMR(∥) = 9125 Oe > HFMR(⊥) = 5897 Oe). Although the study provides valuable insights for the design and optimization of magnetic materials for various technological applications in the field of magnetism, its limitation should be acknowledged. The research did not deeply explore the correlations between the different studied properties, leaving a gap in our overall understanding of these characteristics. Therefore, future work will focus on conducting simulations and theoretical modeling to address this research gap.

Keywords Nd_3Fe_{29} compound · Nd-Fe-based films · Ferromagnetic resonance · X-ray photoelectron spectroscopy (XPS) analysis · Advanced magnetic materials

1 Introduction

In recent years, magnetic materials have garnered significant interest due to their widespread applications in various technological sectors [1–5]. Among these materials, nanocrystalline alloys based on rare earths and transition metals, especially Nd-Fe alloys, have received special attention due to their exceptional magnetic properties and potential for high-performance applications [6–10]. Extensive research has been conducted on the properties of Nd-Fe-based films. For instance, a study by Taylor et al. [11] investigated the influence of deposition parameters on the magnetic characteristics of thin NdFe films deposited on silicon substrates.

✉ R. Fersi
riadh.fersi@fst.utm.tn

[1] LMOP, LR99ES17, Université de Tunis El Manar, 2092 Tunis, Tunisia

[2] Laboratory of Materials Organization and Properties (LMOP), Faculty of Science of Tunis, University of Tunis El Manar, 2092 Tunis, Tunisia

[3] Department of Materials Science and Engineering, 313 Splaiul Unirii Street, 020745 Bucharest, Romania

The results demonstrated that the chemical composition and crystalline orientation of the film could be controlled by adjusting deposition parameters, significantly impacting its magnetic properties. In another research conducted by Suzuki et al. [12], the magnetic anisotropy properties of thin NdFe films were explored concerning film thickness. Researchers observed that the orientation of magnetic anisotropy could be reversed by modulating the film thickness, providing promising prospects for reversible magnetic device design. Moreover, a recent study by Pan et al. [13–15] examined the magnetic properties and thermal stability of Nd-Fe-based films deposited on various substrates. The results revealed that optimizing grain size and film composition led to exceptional magnetic performance and high thermal stability. The microstructure of thin films plays a crucial role in determining their magnetic properties, underscoring the importance of studying and understanding the correlation between microstructural features and magnetic behaviors. Pan Guo-hong et al. [16] achieved a coercivity level of 730 Oe and a saturation magnetization of 20 emu/g in NdFe films cultivated on glass substrates. Croat et al. [15] employed melt-spinning techniques to yield a notable coercivity of 2.1 kOe for $Nd_{1-x}Fe_x$ alloys (with $x = 0.6$). Additionally, Jian et al. [17] demonstrated an impressive coercivity value of 16.8 kOe for $Nd(Fe,Ti)_{12}N_x$ films fabricated via direct current magnetron sputtering on heated Si(1 0 0) substrates. Additionally, the choice of the substrate on which films are deposited can significantly influence their crystalline structure and magnetic response. In this regard, MgO has emerged as a highly favored substrate material due to its excellent lattice match with rare earth and transition metal alloys [18]. This characteristic creates a conducive environment for epitaxial growth, potentially enhancing the magnetic performance of films. Our study findings reveal that Nd_3Fe_{29} alloys exhibit remarkable magnetic properties, including a high Curie temperature (Tc), pronounced magnetic anisotropy (Ha), and significant saturation magnetization (Ms) (Section III.1). These characteristics make these alloys promising candidates for myriad applications in advanced magnetism, spintronics, and information storage devices. Our findings broaden exciting prospects for exploiting these alloys in emerging magnetic technologies and integrating them into high-performance devices. The fundamental objective of this article is to explore and elucidate the microstructural and magnetic properties of Nd3Fe29-based films deposited on MgO (001) substrates and to gain a detailed understanding of how these properties evolve based on preparation conditions: film thickness, annealing temperature, etc. This study encompasses the fabrication of nanocrystalline NdFe/MgO (001) thin films using ultra-high vacuum magnetron sputtering, followed by their characterization using various analytical tools. Building upon previous research, our approach aims to deepen our understanding of these promising materials. In this pioneering study, we conducted a thorough analysis of crucial aspects related to the structure, microstructure, and magnetic properties of Nd3Fe29 compound. Our investigation focused on the meticulous characterization of the microstructure and magnetic attributes of NdFe/MgO (001) thin films prepared by evaporation from nanocrystalline Nd3Fe29 powder. In this context, we scrutinized the magnetic structure of these films in detail, specifically emphasizing their magnetic properties and ferromagnetic resonance phenomena. Utilizing advanced methodologies, we meticulously examined the microstructural and magnetic properties of NdFe/MgO (001) films, evaluating their response to varying thicknesses and thermal treatments. Additionally, a thorough analysis using X-ray photoelectron spectroscopy (XPS) was undertaken to probe the NdFe/MgO (001) films, thus revealing crucial insights into atomic diffusion occurring between the NdFe layer and the tantalum (Ta) capping layer during high-temperature thermal treatments. These aspects encapsulate the essence of our research and significantly contribute to a profound understanding of the complex interplay between microstructure and magnetic properties in the context of NdFe/MgO (001) films.

The results obtained in this study have highlighted the effectiveness of several parameters in increasing reaction yields. Firstly, the use of a continuous magnetic sputtering system under ultra-high vacuum conditions allowed precise control of the composition and structure of the films. This precision is crucial as the magnetic properties of films depend closely on their composition and structure. Furthermore, the adoption of a nanocrystalline Nd3Fe29 alloy target favored the creation of films with a more uniform grain size. A uniform grain size is crucial for the magnetic properties of films as it reduces defects and impurities. Finally, employing a variable-temperature annealing process improved the crystallinity and microstructure of the films. This enhancement resulted in a significant increase in coercivity (Hc), magnetic remanence (Mr), and magnetic anisotropy (Ha) of the films.

2 Experimental procedure

In the present study, we synthesized NdFe/MgO(001) films of varying thicknesses using a direct current magnetron sputtering system in ultra-high vacuum conditions at room temperature, maintaining a base pressure of approximately 1×10^{-5} Pa. The depositions were performed on MgO

(001) substrates, employing a nanocrystalline Nd3Fe29 alloy target. Preceding the deposition, the nanocrystalline Nd3Fe29 powder target was prepared through a high-energy ball milling process lasting 5 h, conducted under a high-purity argon atmosphere. Subsequently, the Nd3Fe29 samples (Numéro CAS (Nd): 7440–00-8, Numéro CAS (Fe): 7439–89-6) underwent a 30-min annealing process within a sealed silica tube under 10^{-6} Torr, at various annealing temperatures (Ta) ranging from 600 to 1750 K. To prevent oxidation of the NdFe/MgO(001) films in ambient air, a thin tantalum (Numéro CAS (Ta): 7440-32-6) capping layer with a thickness of 10 nm was deposited. The NdFe/MgO(001) films were subsequently subjected to annealing at different temperatures (T_a) spanning from 573 to 1173 K for an hour within the same chamber, maintaining a base pressure of approximately 1×10^{-4} Pa. The crystallinity and microstructure of the films were meticulously analyzed utilizing grazing-incidence X-ray diffraction (GIXRD) techniques. For the examination of film morphology, a scanning electron microscope (SEM) on a JSM7100 was employed. The film composition was determined through X-ray photoelectron spectroscopy (ESCALAB 250Xi) and energy-dispersive X-ray spectroscopy (EDX) coupled with scanning electron microscopy (SEM). Surface roughness parameters (Rrms) and grain size (Φ) were evaluated using atomic force microscopy (AFM, model 3SPA-300HV). The magnetic properties of the films were characterized at room temperature using a vibrating sample magnetometer (VSM). Measurements were carried out with a magnetic field applied both parallel and perpendicular to the film plane, enabling the evaluation of parameters such as coercivity (Hc), remanent magnetization (Mr), and magnetic anisotropy (Ha). Concurrently, ferromagnetic resonance (FMR) measurements were conducted employing a Bruker EMX model X-band electron paramagnetic resonance spectrometer at a microwave frequency of 24 GHz. This comprehensive experimental procedure facilitated a detailed investigation into the microstructural and magnetic attributes of the NdFe/MgO(001) thin films, enabling a robust foundation for subsequent analysis and interpretation. A triple monochromator Raman spectrometer utilizing a krypton-ionized CRL 62 laser with a wavelength of 65 Ångströms and a power of 300 mW was employed. This polarized Raman spectroscopy study was conducted on a single crystal, enabling the assignment of each peak to a vibration mode based on the polarization state. The process flow diagram for the elaboration and characterization of our films is presented below.

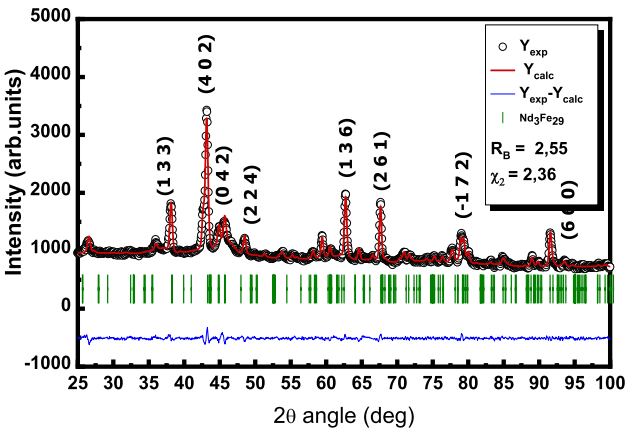

Fig. 1 Rietveld analysis for X-ray diffraction pattern of Nd3Fe29 compound annealed sample at 1073 K

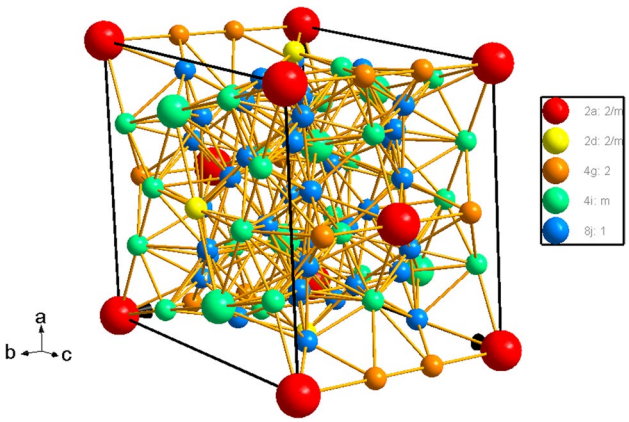

Fig. 2 Crystal structure of Nd_3Fe_{29} compound

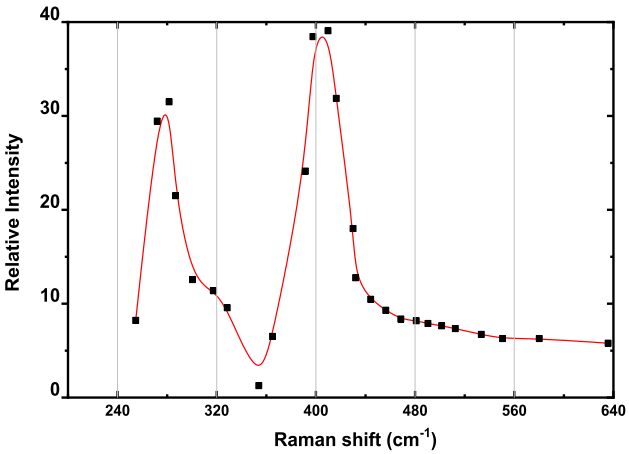

Fig. 3 *Spectres Raman* of Nd_3Fe_{29} compound annealed sample at 1073 K

1. Preparation of Nd_3Fe_{29} Target Material

- High-energy milling under argon atmosphere for 5 hours

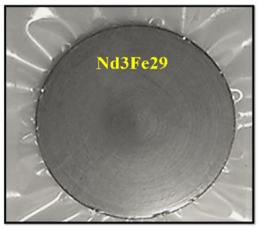

Nd3Fe29 Target prepared by arc furnace

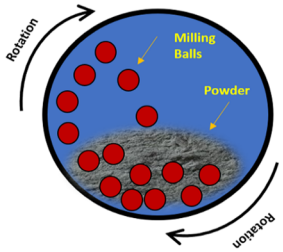

2. Nd_3Fe_{29} powder Analysis

- X-ray Diffraction Analysis
- Raman Spectrum Analysis

3. Deposition of NdFe/MgO(001) Films on MgO(001) Substrates

- Use of nanocrystalline Nd3Fe29 source
- Utilization of ultra-high vacuum magnetron sputtering system
- Deposition at different annealing temperatures (Ta)
- Deposition of a 10 nm thick tantalum (Ta) layer to prevent oxidation

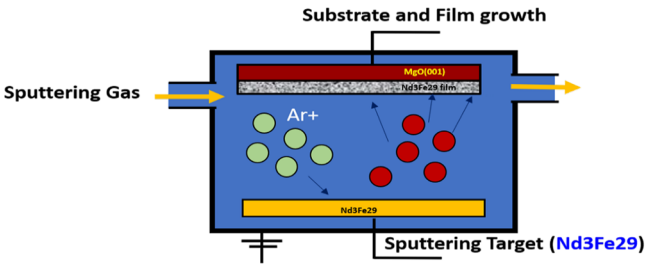

4. Annealing of NdFe/MgO(001) Films

- At various temperatures (Ta) within the same chamber
- Maintaining a base pressure of approximately 1×10^{-4} Pa

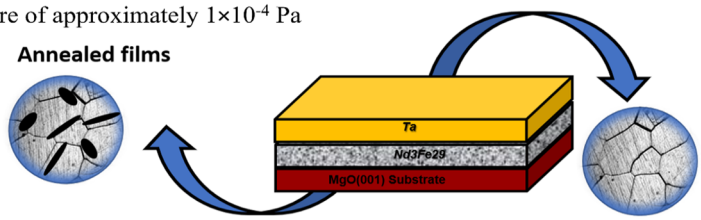

5. Film Analysis

- GIXRD for crystallinity and microstructure
- SEM for morphology/XPS and EDX for chemical composition
- AFM for surface roughness parameters (R_{rms}) and grain size (Φ)
- VSM for magnetic properties / FMR for ferromagnetic resonance measurements

6. End of the Experiment

End

3 Results and discussion

3.1 Structure, microstructure and magnetic properties of Nd_3Fe_{29} compound

The results of the Rietveld refinement of X-ray diffraction (XRD) with CuKα radiation on a Bruker D8 powder apparatus for the Nd3Fe29 samples annealed at 1073 K are depicted in Fig. 1. These analyses have provided us with an intricate insight into the crystalline structure of the sample, enabling us to accurately characterize its structural properties.

The results of the structural refinement have revealed the presence of a main phase exhibiting a monoclinic structure, attributed to the C2/m space group. The lattice parameters were determined with high precision, displaying values of a = 9.71 Å, b = 8.58 Å, and c = 10.51 Å. The angles α, β, and γ were measured as 90.00°, 96.15°, and 90.00° respectively, confirming the monoclinic nature of the crystalline structure. Atomic positions were identified within this configuration. Nd atoms occupy the crystallographic sites 2a (0 0 0) and 4i (0 ½ ½), while Fe atoms are located at sites 2d (0 ½ ½), 4e (¼ ¼ 0), 4 g (0 0.360074 0), 4i (0.208158 ½ 0.859961), 4i (0.979024 ½ 0.748184), 4i (0.219787 ½ 0.106261), 4i (0.59553 ½ 0.29068), 8 g (0.93637 0.252535 0.596249), 8 g (0.909013 0.774722 0.196093), 8 g (0.814904 0.645351 0.375092), and 8 g (0.155881 0.747002 0.197647) (Fig. 2). To assess the goodness-of-fit of the Rietveld refinement, the R-factor (R_a) and the χ^2 value were examined. These parameters serve as measures of the agreement between the experimental results and the refinement data. The RB and χ^2 values, presented in an inset in Fig. 1, were scrutinized to ensure the reliability of the refinement results and confirm the correspondence of the obtained crystalline structure with the experimental data. The Raman analysis of the Nd_3Fe_{29} compound annealed sample at 1073 K (Fig. 3) revealed the presence of characteristic bands. The most intense band, at 441 cm^{-1}, is attributed to the octahedral deformation vibration of Fe atoms. Another significant band, at 272 cm^{-1}, is attributed to the tetrahedral deformation vibration of Nd atoms. The presence of these Raman bands confirms the monoclinic structure of the Nd3Fe29 sample. The lattice parameters a = 9.71 Å, b = 8.58 Å, and c = 10.51 Å, along with the angles α, β, and γ of 90.00°, 96.15°, and 90.00°, were determined through Raman analysis. Furthermore, the Raman analysis identified the atomic positions of Nd and Fe in the crystalline structure. These results corroborate the findings obtained from X-ray diffraction.

Figure 4(a) illustrates the magnetization curve as a function of temperature (M(T)) for the Nd3Fe29 compound. The Curie temperature (T_C) is estimated to be around 388 K, indicating the magnetic stability of this compound at relatively high temperatures. In pursuit of optimizing the extrinsic magnetic properties of the Nd3Fe29 compound, such as coercivity (Hc), remanent magnetization (Mr), and the maximal energy product ((BH)max), we conducted various annealing treatments at different temperatures (Ta) for this material. Figure 5(a) presents the evolution of these extrinsic magnetic properties (coercivity (Hc)), remanent magnetization (Mr)) as a function of annealing temperature (Ta). The results demonstrate that the optimal extrinsic magnetic performance is achieved at an annealing temperature of Ta = 1073 K: Hc = 18,326 Oe, Mr = 48.52 emu/g, and $(BH)_{max}$ = 9.25 MGOe. Additionally, Fig. 4(b) illustrates the hysteresis loop at 298 K for the nanocrystalline Nd3Fe29 sample annealed at 1073 K, exhibiting a grain size closest to the desired optimal diameter (≃ 90 ± 2 nm). To achieve magnetization saturation, a magnetic field (H) ranging from − 90,000 Oe to + 90,000 Oe was applied, as depicted in Fig. 4(b) for the nanocrystalline Nd3Fe29 compound annealed at Ta = 1298 K. The magnetization curves (M(H)), represented by solid lines, were extracted from experimental data, and theoretical fitting was performed using the saturation approach law described in references [19, 20]. The values of saturation magnetization (Ms) and anisotropy field (Ha) were assessed. The magnetic anisotropy of 100,000 Oe suggests that Nd3Fe29 alloys exhibit a strong preference for a specific magnetization direction, which is pivotal for numerous applications requiring unidirectional magnetization. We found an Ms value of 71 emu/g for Nd3Fe29 alloys, signifying their high magnetization capacity at full saturation. These magnetic characteristics render Nd3Fe29 alloys highly promising for diverse applications in the field of magnetism.

3.2 Microstructure and magnetic properties of NdFe/MgO (001) films

The grazing incidence X-ray diffraction (GIXRD) results of the NdFe/MgO (001) films with various thicknesses, annealed at 773 K for 1 h, are presented in Fig. 6. These films were elaborated by evaporation from Nd3Fe29 nanocrystalline powder annealed at 1073 K. When the films had a thickness of 20 nm, a low diffraction intensity corresponding to the (402) plane of Nd3Fe29 was observed, accompanied by a broad amorphous peak at 43.5°, revealing their nanocrystalline nature. This feature indicates that the films consist of small-sized grains and possess a disordered atomic-scale structure. As the thickness t reaches 100 nm, more significant changes become evident. The diffraction peaks exhibit an overall reduced intensity and noticeable broadening, suggesting a larger distribution of grain sizes and potential residual stresses resulting from growth. At a thickness of 200 nm, the diffraction peaks reveal a series of sharp

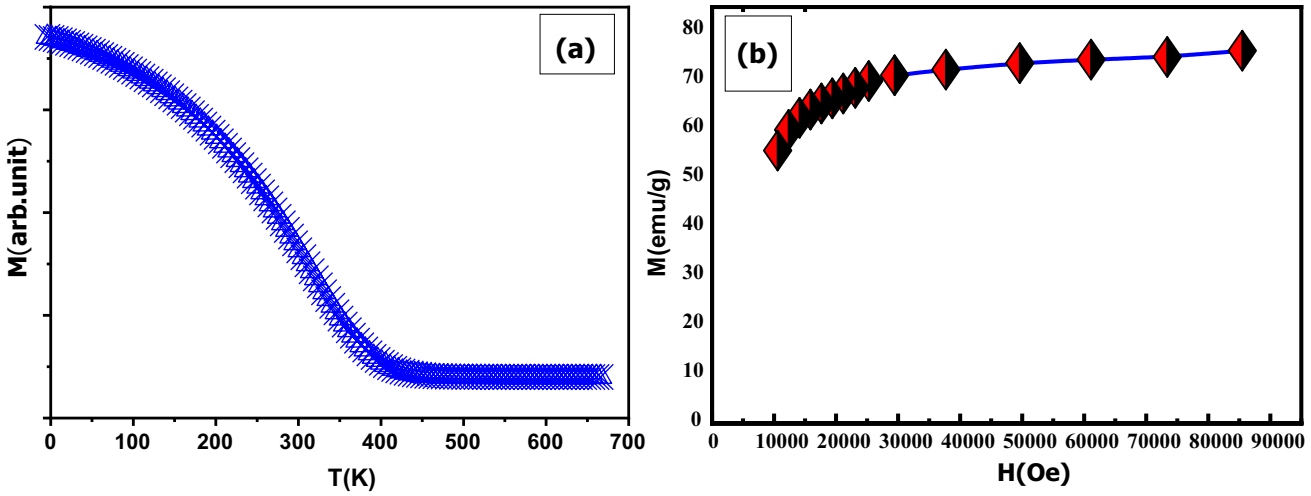

Fig. 4 **a** Magnetization curves M(H) of Nd_3Fe_{29} compound annealed sample at 1073 K. **b** The magnetization curve M(H) of the nanocrystalline Nd3Fe29 compound annealed 1298 K. The applied magnetic field H between − 90,000 Oe and + 90,000 Oe. The solid lines show the experimental measurement data and the fit given by the theory using the saturation approach law expression [19, 20]

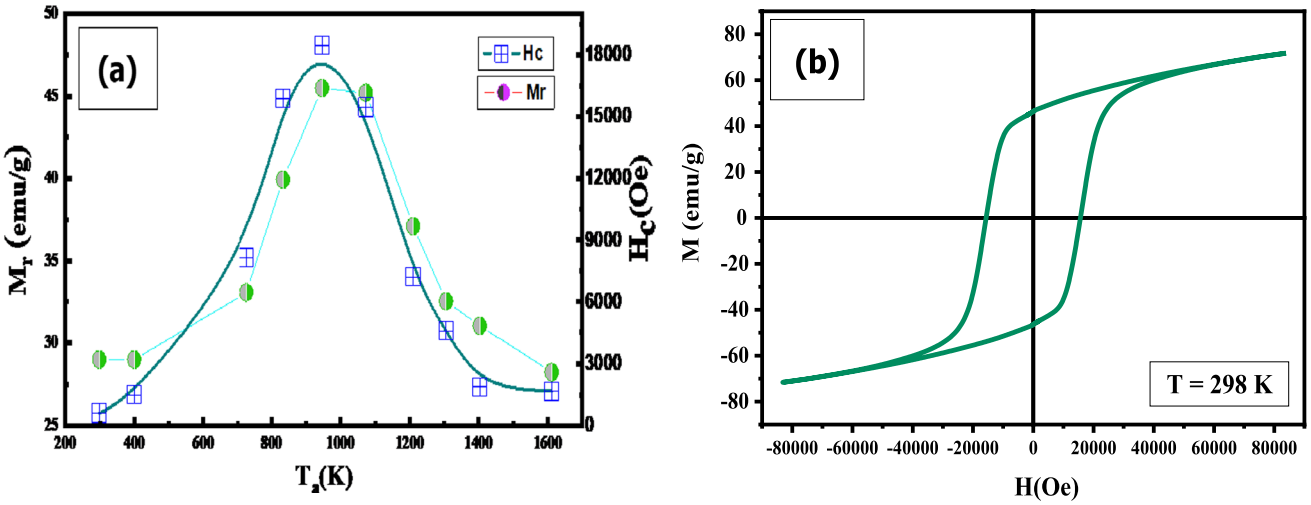

Fig. 5 **a** Evolution of extrinsic magnetic properties Mr (remanence magnetization) and Hc (coercivity) as a function of annealing temperature Ta. **b** Hysteresis curves of nanocrystalline Nd3Fe29 compound annealed at $T_a = 1073$ K, measured at 298 K

and intense crystalline reflections. These peaks indicate a well-ordered crystalline structure, suggesting preferential growth in certain crystallographic orientations. As the thickness increases to 250 nm, the diffraction peaks display slight broadening and a slight decrease in intensity. This could indicate a relaxation of crystalline stresses due to growth, accompanied by a slight increase in the size of crystalline grains. As the thickness further increases to 300 nm, the diffraction peaks become broader and more diffuse, indicating an increased dispersion of crystallographic orientations and larger grain size. At a thickness of 400 nm, a partial reappearance of diffraction peak intensity is observed, which might suggest a partial restoration of crystalline order at this thickness. This phenomenon could be attributed to recrystallization processes or changes in growth conditions. The analysis by Grazing Incidence X-ray Diffraction (GIXRD) highlighted the presence of peaks corresponding to traces of magnesium oxides on the surface of the MgO substrate. This formation of magnesium oxides results from the oxidation of the MgO (001) substrate surface upon exposure to oxygen or ambient air humidity. Furthermore, the presence of traces of iron (III) oxides (Fe2O3) was identified. This formation arises from the reaction between the iron content in the NdFe alloy and the surrounding oxygen. Similarly, XRD analysis revealed the presence of peaks corresponding

to neodymium oxide (Nd2O3), attributable to the reaction of neodymium present in the NdFe alloy with oxygen.

Furthermore, in order to better characterize the crystallization quality of the NdFe/MgO (001) films, we estimated the average grain size using the Scherrer equation [21, 22], based on the width of the (220) diffraction peak. The results revealed a significant increase in the average crystallite size with the increase in the thickness of the NdFe films. Specifically, for films with a thickness of 20 nm, the average crystallite size was estimated to be around 8 nm, while for films with a thickness of 100 nm, it had increased to about 30 nm. This positive evolution indicates a progressive improvement in crystallization quality with increased film thickness, attesting to a more regular structure and improved atomic coherence. Scanning Electron Microscopy (SEM) images of the NdFe/MgO (001) films with different thicknesses, vacuum annealed at 873 K for 1 h, are presented in Fig. 5. When the NdFe/MgO films had a thickness of 20 nm, the presence of small uniform crystallites was observed. These small uniform crystallites correspond to the nanocrystalline nature of the NdFe/MgO (001) films. With the increase in thickness of the NdFe/MgO (001) films to 50 nm, a notable increase in the quantity of crystallites in the NdFe layer was observed. This increase is attributed to the enhancement of film crystallization at this thickness. When the NdFe/MgO (001) films had a thickness of 50 nm and 300 nm, a clear growth of a large number of crystallites in the NdFe layer was observed. The average size of these crystallites was estimated to be about 30 nm (Fig. 7b) and 80 nm (Fig. 7c), respectively. The higher values estimated from the SEM images for larger crystallites are attributed to the coalescence of NdFe grains. This indicates that individual NdFe grains aggregated to form larger crystallites, thus leading to an observed increase in average size. These observations confirm that film thickness has a significant influence on the crystallization and size of the NdFe layer crystallites, which can be crucial for tailoring film properties for their potential applications. Additionally, Fig. 8a–b presents Atomic Force Microscopy (AFM) images of the NdFe/MgO (001) films. We also estimated the surface roughness (R_{rms}) of the films from these topographical images, obtaining values ranging from 2.69 nm for t = 20 nm (a) to 11.72 nm for t = 400 nm (b). These roughness measurements complement the information about the surface quality of the NdFe/MgO (001) films, revealing significant variations across the different studied thicknesses.

The results of our study reveal a significant variation in the defect density within NdFe/MgO (001) films depending on the annealing atmosphere. Under a high-purity argon atmosphere (Ar HP), we observed a relatively low defect density, indicating increased crystallinity and a more homogeneous structure within the films. However, this finding was drastically altered when the argon ratio (Ar) was increased, leading to a significant increase in the defect density. Furthermore, our analysis at different annealing temperatures revealed crucial trends. At an initial temperature of 573 K, the defect density was at its minimum, suggesting that the films exhibited a more stable crystalline structure with fewer apparent crystalline defects. However, as the annealing temperature increased, we observed a progressive increase in the defect density. At 873 K, this trend became significantly pronounced, with a marked increase in dislocation density, highlighting the films' sensitivity to temperature. Eventually, at the maximum annealing temperature of 1173 K, the defect density had reached its peak, marked by a profusion of dislocations and other crystalline defects. These results clearly illustrate the influence of the annealing atmosphere on the

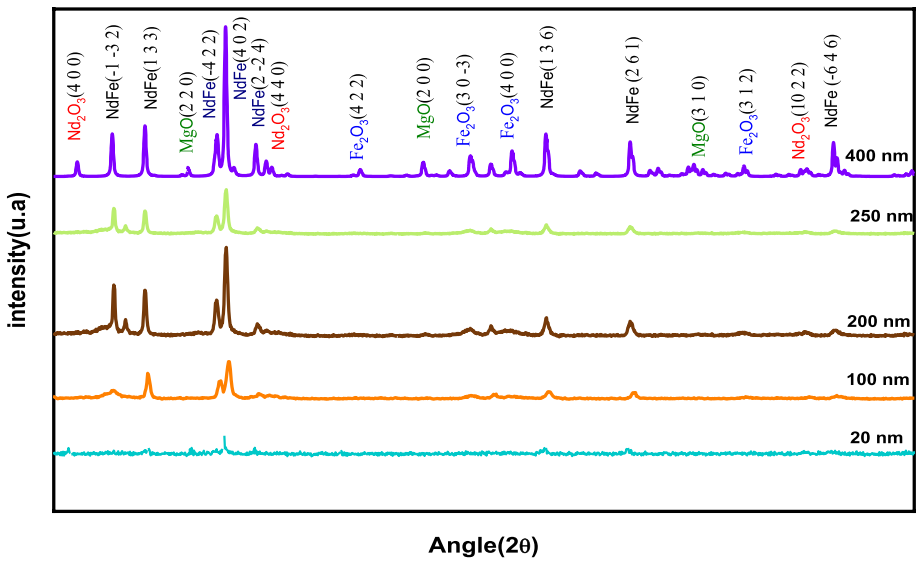

Fig. 6 Grazing Incidence X-ray Diffraction (GIXRD) patterns for nanocrystalline NdFe/MgO(001) films with different thicknesses: t = 20 nm, 100 nm, 200 nm, 250 nm, and 400 nm, annealed at 873 K for 1 h

defect density, as well as the dependence of this density on the annealing temperature.

3.3 Magnetic structure of NdFe/MgO (001) films

The images obtained through Magnetic Force Microscopy (MFM), as depicted in Fig. 9, unveil a captivating perspective of NdFe/MgO (001) films with varying thicknesses: t = 50 nm (a), t = 250 nm (b), t = 400 nm (c), annealed at 873 K for 1 h. A meticulous analysis of these MFM images reveals striking contrasts, highlighting the presence of magnetic domains on the surface. Each magnetic domain is carefully demarcated by well-defined boundaries, attesting to a precise organization of the magnetic structure at the microscopic scale. Upon exploring films with thicknesses ranging from 20 to 150 nm, a noteworthy observation emerges: the surface is adorned with a multitude of uniform magnetic domains. This uniformity suggests a remarkable crystallization process and an ordered arrangement of magnetic grains within this range of thicknesses. However, at a thickness of 20 nm, an intriguing observation takes center stage. The MFM image unveils a complex pattern of undulating domains. This peculiarity could stem from a diminished contribution of magnetic moments at the surface, perhaps owing to the nanoscale dimension of the magnetic grains [23]. These reduced dimensions might induce specific

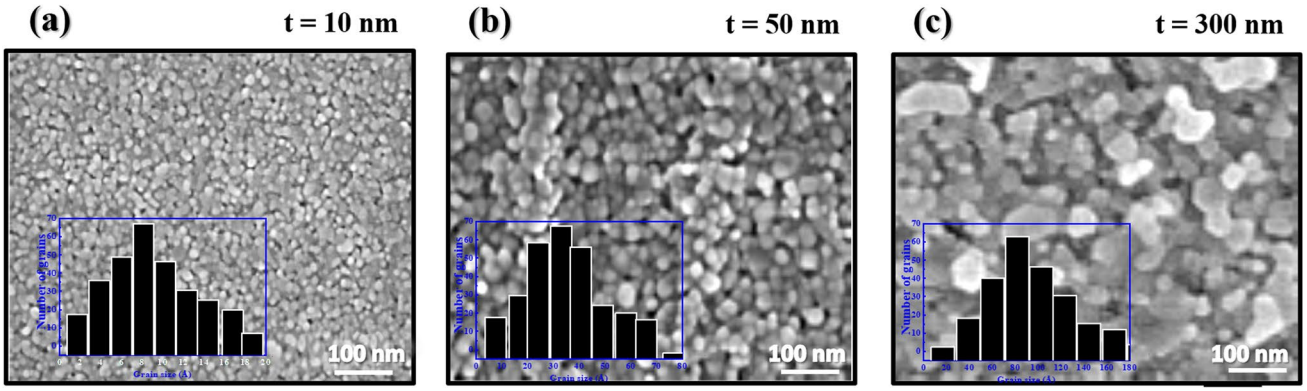

Fig. 7 Scanning Electron Microscopy (SEM) images of NdFe/MgO(001) films with different thicknesses annealed at a temperature of 873 K for 1 h: **a** 20 nm, **b** 50 nm, and **c** 300 nm

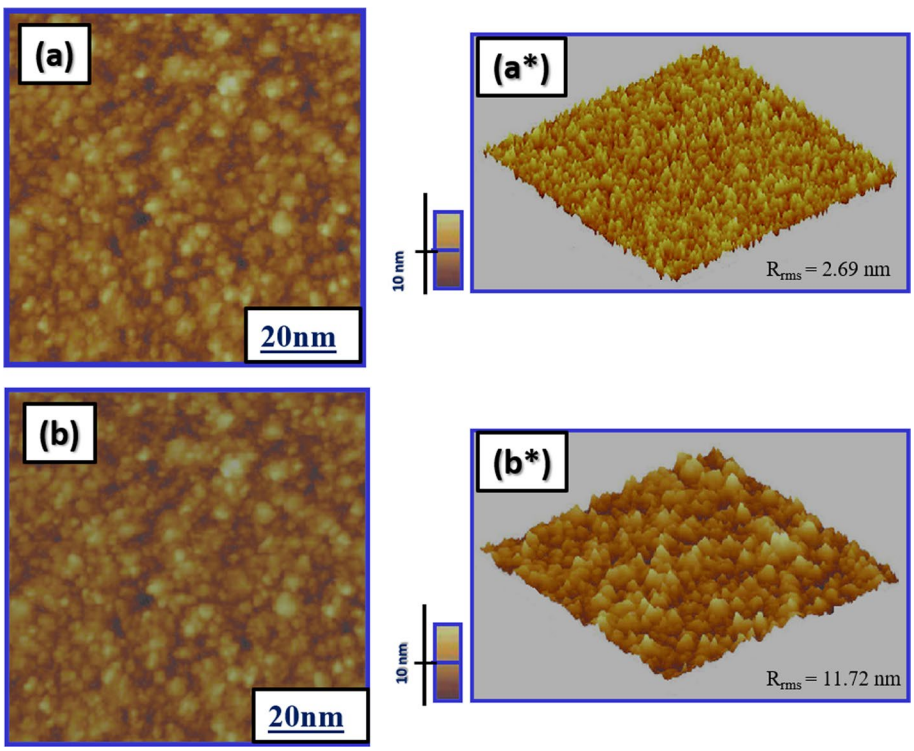

Fig. 8 AFM topographic images for nanocrystalline NdFe/MgO(001) films with different thicknesses: t = 20 nm (**a**) and t = 400 nm (**b**), annealed at a temperature of 873 K for 1 h

magnetic interactions, adding an additional layer of complexity to the configuration. In contrast, at a thickness of 250 nm, an entirely different perspective emerges. Unique domains, ranging in size from 5 to 15 µm, come into view, indicating an even more complex organization of magnetic grains at this thickness. This heightened complexity could arise from a delicate balance between magnetic anisotropy and the interaction energy between the grains. One could envision these configurations as the result of a subtle dance between these factors. For films with a thickness equal to or greater than 300 nm, an additional evolution becomes apparent. The magnetic domains increase in scope, suggesting an augmentation in the size of magnetic grains in a state characterized by multiple magnetic domains. This evolution could be attributed to the coalescence of magnetic grains, which come together to form larger and harmonious magnetic domains.

3.4 Magnetic properties and ferromagnetic resonance of NdFe/MgO (001) films

Ferromagnetic Resonance (FMR) spectra of NdFe/MgO (001) films annealed at 873 K for 1 h are shown in Fig. 10, providing a detailed overview of the effects of different thicknesses t = 20 nm, 100 nm, 200 nm and 400 nm. These measurements were meticulously conducted under the influence of magnetic fields oriented both parallel (∥) ($\theta_H = 90°$) and perpendicular (⊥) ($\theta_H = 0°$). To gain comprehensive insights into the HFMR resonance fields, the FMR spectra were rigorously fitted using a Lorentzian profile (depicted by the navy blue line), based on the double-fold anisotropy model proposed by Chappert [24]. A meticulous analysis of the $H_{FMR}(\theta_H)$ curve unveils a distinct predominance of a perpendicular easy axis (⊥), where the resonance fields reach minimal values such as 334.1 Oe for δ = 20 nm, 385.2 Oe for t = 100 nm, 638.5 Oe for t = 300 nm, and 907.3 Oe for t = 400 nm. Conversely, the hard axis aligns parallel (∥) to the film plane, thus exhibiting the maximum value of the HFMR resonance field, namely 756.8 Oe for t = 20 nm, 790.3 Oe for t = 100 nm, 922.3 Oe for t = 300 nm, and 506.7 Oe for t = 400 nm. The illustration of the angular evolution θ_H of the H_{FMR} resonance field is presented in Fig. 9. The values of saturation magnetization Ms, as well as the anisotropy field Ha, were precisely determined for all films, relying on the Kittel equations described in reference [25, 26]. The magnetocrystalline anisotropy is in perfect correlation with the behavior of K_1. K_1 turns out to be positive only when the thickness is below 300 nm, under a condition where $K2 > -K_1$, favoring an easy magnetization axis aligned parallel (∥) to the film plane, in opposition to shape anisotropy. For films with thickness t = 400 nm, the resulting anisotropy constants manifest as follows: $K_1 = -0.18 \times 10^8$ erg/cm^3 (− 18,000 J/m^3) and $K_2 = 1.21 \times 10^8$ erg/cm^3 (121,000 J/m^3). The positivity of K_2 with $K_1 > -K2$, coupled with the configuration of the $H_{FMR}(\theta_H)$ curve where H_{FMR} (∥) = 506.0 Oe < H_{FMR} (⊥) = 797.0 Oe, strongly suggests that the easy axis aligns perpendicular (⊥) to the plane of the NdFe/MgO (001) films. The values of Ms H_{FMR} (⊥), H_{FMR}(∥), ($\theta°_u$), and Ha as a function of thickness t are indicated in Table 1. The predominance of a perpendicular easy axis in the H_{FMR} resonance curves for the thinner thicknesses is coherent with the perpendicular magnetic domains observed in the MFM images. The increase in film thickness leads to significant changes in the resonance fields, which can be attributed to the complex variations in the arrangement of magnetic domains as the dimensions of the magnetic grains and their interactions evolve [27]. By combining the MFM observations with the ferromagnetic resonance (FMR) measurements, a clear correlation emerges: the microscopic features of the magnetic domains visualized by MFM are closely related to the magnetic resonance properties measured by FMR. The details observed in the MFM images, such as uniform magnetic domains at certain thicknesses and wavy patterns at others, find their echo in the variations of resonance fields and easy axes observed in the H_{FMR} resonance curves.

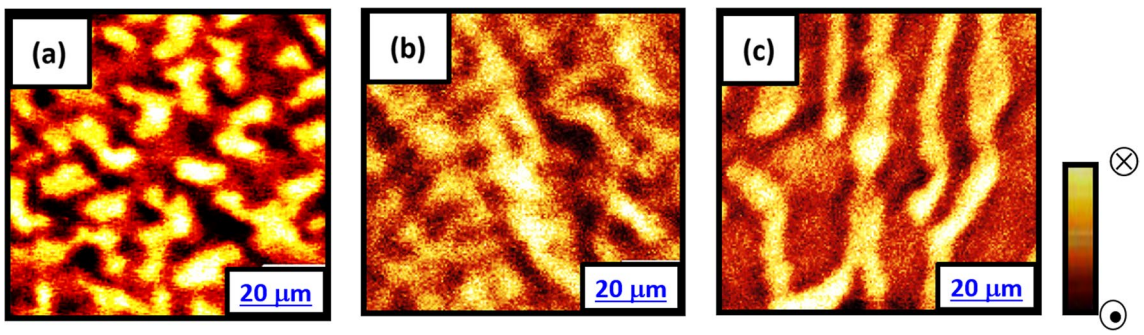

Fig. 9 Images obtained from Magnetic Force Microscopy (MFM) of NdFe/MgO(001) films with different thicknesses: t = 50 nm (**a**), t = 250 nm (**b**), t = 400 nm (**c**), annealed at 873 K for 1 h

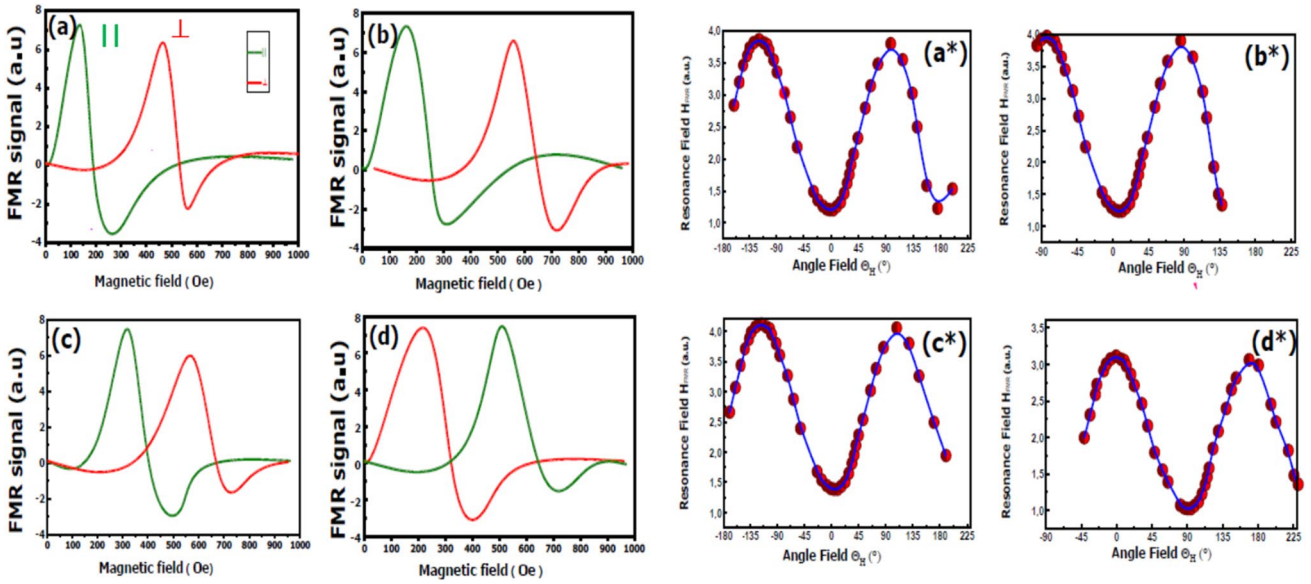

Fig. 10 **a** FMR measurements performed on the NdFe/MgO(001) films: FMR signals under parallel (∥) (θH = 90°, green line) and perpendicular (⊥) (θH = 0°, violet line) magnetic field, for t = 20 nm (**a**), 100 nm (**b**), 250 nm (**c**), and 400 nm (**d**), annealed at 873 K for 1 h. Angular variations θH of the resonance field HFMR. The navy line presents the simulation of FMR measurements using Chappert model [24]

Figure 11 presents the hysteresis loops at room temperature measured by applying a perpendicular (⊥) magnetic field to the plane of the NdFe/MgO (001) films with different thicknesses, which underwent annealing at 773 K for 1 h. Table 1 shows the dependence of the values of Ms (saturation magnetization) and Hc (coercivity) on the film thickness. When the NdFe/MgO (001) films had a thickness of 20 nm, a low Ms value of 169 emu/cm^3 was observed due to their nanocrystalline nature. This reduced Ms value is a result of the grains in the NdFe layer likely being in a single-domain state, given their small size (less than 15 nm). In a single-domain state, magnetization reversal occurs through the rotation of all magnetic moments as a unit, requiring dominant anisotropy energy. However, with the increase in the thickness of the NdFe/MgO (001) films to 300 nm, the Ms value gradually increased to 397 emu/cm^3. This increase in Ms can be attributed to several factors. Firstly, the average grain size increased to 80 nm for the 300 nm films, favoring a multi-domain state. In a multi-domain state, magnetization reversal occurs through domain wall motion, requiring less energy than in a single-domain state. Additionally, at a thickness of 250 nm, the maximum Hc value of 5230 Oe was observed. This increase in coercivity (Hc) at 250 nm can be explained by a change in grain size and domain state [28]. Below this thickness, the films were likely in a single-domain state, resulting in relatively low coercivity. However, at a thickness of 300 nm, the films reached a state where the multi-domain state was favored, leading to a significant reduction in coercivity (Hc). Previous studies have demonstrated that surface roughness can have a significant impact on the magnetic properties of materials. By increasing the film thickness and thus the surface roughness, we observed a corresponding modification of the magnetic properties of the studied films. These variations suggest a direct influence of surface morphology on the magnetic structure of the films [29, 30].

Table 1 The magnetic parameters of nanocrystalline NdFe/MgO (001) films recuits à une température à 873 K pendant 1 heure, for different t thickness, obtained by FMR measurements: Ms(emu/cm^3), H_a (Oe), H_{FMR} (∥) (Oe), H_{FMR} (⊥) (Oe), easy axis direction (θ◦u) and Hc(Oe), Mr(emu/cm^3)

t(nm)	20	50	100	150	200	250	300	350	400
M_s	169	214	298	352	397	396	357	320	267
$H_{FMR}(\perp)$	3330	3425	3850	3956	4892	5897	6380	7898	9070
$H_{FMR}(\parallel)$	7560	7589	7903	8569	8978	9125	9220	8975	5060
H_a	9023	9027	9856	10,024	10,478	10,325	10,201	9856	9547
(θ°_u)	0	0	0	0	0	0	90	90	90
H_c	2456	2789	3268	3545	4897	5230	3125	3002	2125
Mr	175	189	192	197	201	211	210	195	182

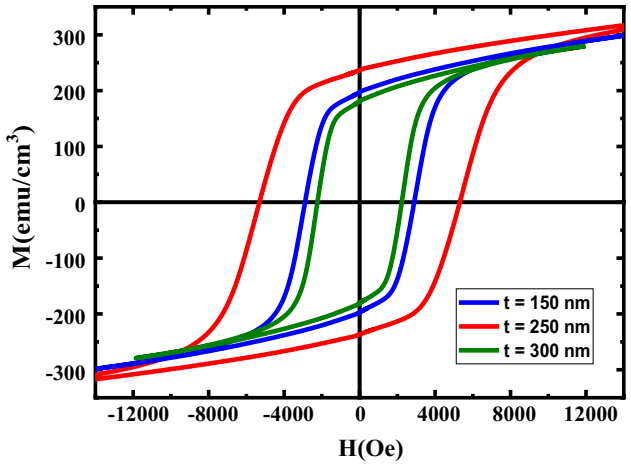

Fig. 11 Hysteresis loops of NdFe/MgO(001) film for different t thickness (t = 150 nm, 250 nm and 300 nm) annealed at 873 K

Figure 12 highlights the hysteresis loops of the NdFe/MgO (001) films with a thickness of 200 nm, annealed at various temperatures ranging from 573 to 1173 K. Table 2 presents the variation of Hc (coercivity) and Ms (saturation magnetization) values as a function of annealing temperature (Ta). When the NdFe/MgO (001) films were annealed at 673 K, a low Ms value of 212 emu/cm^3 is observed. This low value indicates the coexistence of an amorphous phase with a small amount of nanocrystalline NdFe in the films. However, as the annealing temperature increases, the NdFe grains experience improved crystallization and increased ordering, leading to a progressive increase in the Ms value. At 873 K, after annealing, the Ms value reaches 582 emu/cm^3, illustrating a significant enhancement in the magnetic properties. However, an intriguing observation is made during annealing at 1173 K, where the Ms value does not continue to increase but decreases to 421 emu/cm^3. This decrease is most likely due to intermixing between the NdFe layer and the tantalum (T_a) layer at high temperatures. The interaction between these layers can lead to changes in magnetic properties, hence the unexpected decrease in Ms. Concurrently, the value of coercivity (Hc), which measures resistance to demagnetization, also shows a significant evolution with annealing temperature. At 573 K, the coercivity Hc is relatively low at 1268 Oe, but at 873 K, the coercivity Hc increases substantially to 5230 Oe. This increase is attributed to the more advanced crystallization and ordering of the NdFe/MgO (001) films at higher temperatures, enhancing their resistance to demagnetization.

It is essential to note that the outstanding magnetic properties observed in the 250 nm-thick NdFe/MgO (001) film after annealing at 873 K are comparable to those reported in previous studies on NdFe-based films. For instance, in the work by Pan Guo-hong and his team, a coercivity of 730 Oe and a saturation magnetization (Ms) of 20 emu/g were measured for NdFe films grown on glass substrates [13]. Croat et al. [15] achieved a high coercivity (Hc) of approximately 2.1 kOe for $Nd_{1\_x}Fex$ alloys obtained by melt-spinning, with x = 0.6. M. R. Jian et al. [17] demonstrated that $Nd(Fe,Ti)_{12}N_x$ films, prepared by direct current magnetron sputtering on heated Si(1 0 0) substrates, exhibit a high coercivity value of 16.8 kOe. In our case, the magnetic properties proved even more remarkable: a coercivity of 5230 Oe, a remanent magnetization of 211 emu/cm^3, a magnetic anisotropy field of 10,325 Oe, a saturation magnetization (Ms) of 396 emu/cm^3, and a Curie temperature of approximately 388 K. It is noteworthy that the obtained values are comparable to those of currently highly commercialized films, such as NdFeB and SmCo [31, 32]. These results strengthen the prospect of a promising application for this magnetic film in various technological and industrial fields, such as electric motor manufacturing, electronic devices, and energy storage applications.

3.5 X-ray photoelectron spectroscopy (XPS) analysis of NdFe/MgO (001) films

The results obtained through X-ray Photoelectron Spectroscopy (XPS) provided a precise evaluation of the chemical composition of our samples' surface. Analyzing the intensity of the XPS peaks associated with neodymium and iron allowed for the calculation of the sample's synthetic ratio. It is noteworthy that the composition of the films, as identified by XPS, closely matched that of the target used as the source material. This similarity enabled us to determine the predicted ratio of the synthesized samples, reflecting the proportion between neodymium and iron atoms in the films. Deducing from the intensities of the relevant XPS peaks, the Nd: Fe ratio in the sample was 29% neodymium atoms and

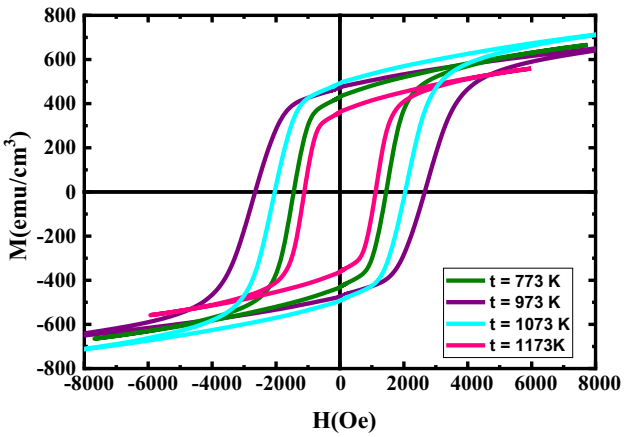

Fig. 12 Hysteresis loops of NdFe/MgO(001) film as a function of annealing température T_a

Table 2 Variation of Hc (coercivity) and Ms (saturation magnetization) values with respect to the annealing temperature (Ta) of NdFe/MgO(001) films

T_a	573 K	673 K	773 K	873 K	973 K	1073 K	1173 K
H_c(Oe)	1268	2545	3598	5230	2125	2178	1925
M_s(emu/cm^3)	302	356	498	582	522	476	421

71% iron atoms, which is close to the ratio of Nd3Fe29. To clarify the interdiffusion phenomenon between the Nd3Fe29 layer and the tantalum (Ta) layer during high-temperature annealing, we subjected the corresponding samples to in-depth analysis using X-ray Photoelectron Spectroscopy (XPS). This technique provides precise information about the elements present on the sample surface and allows determination of their chemical bonding states [27, 33, 34]. Figure 13 illustrates the evolution of the Fe 2p and Ta 4f core level spectra throughout the thermal treatment of NdFe/MgO (001) films, annealed at 1073 K. After this thermal treatment, evident oxidation of the tantalum layer was observed, unequivocally confirming the presence of this material in the sample. Furthermore, the interface between the Ta coating and the NdFe layers remained distinctly visible with sharp clarity. As the number of annealing cycles increased, a significant transformation occurred. The intensity of the Fe 2p1/2 and Fe 2p3/2 peaks gradually increased, while more pronounced Fe 2p1/2 and Fe 2p3/2 peaks appeared during the tenth (10th) annealing cycle (Fig. 13a). Concurrently, the intensity of the Ta 4f 5/2 and Ta 4f 7/2 peaks markedly decreased during the eighth (8th) and tenth (10th) annealing cycles (Fig. 13b). These observations indicate the diffusion of iron (Fe) atoms from the NdFe layer to the upper tantalum (Ta) layer, and vice versa, with tantalum (Ta) atoms from the coating layer also diffusing into the NdFe layer. However, this interdiffusion remained limited, so the interface between the two layers, clearly visible after the eighth annealing cycle, could still be distinctly observed even after the thermal treatment at 1073 K. The results found revealed that the annealing process led to an increase in defect concentration in the studied films. These defects primarily manifest as interstitial oxygen atoms, interstitial iron and tantalum atoms, as well as edge defects. Interstitial oxygen atoms were identified as having a potentially negative effect on the magnetic properties of the films due to their disruption of the crystalline structure of the NdFe material. Additionally, the presence of interstitial iron and tantalum atoms was also associated with disruption of the crystalline structure, contributing to the decrease in saturation magnetization. These defects were clearly detected by analyzing the XPS spectra, where an additional peak appears at a higher binding energy than the peak corresponding to oxygen atoms bound to iron or tantalum atoms. Furthermore, a decrease in the height of the XPS peaks corresponding to atoms from a given layer was also observed, confirming the presence of these defects. Regarding edge defects, their influence was highlighted by promoting atom diffusion between the NdFe and Ta layers, leading to further reduction in saturation magnetization. The presence of these edge defects was also confirmed by a decrease in the height of the XPS peaks corresponding to atoms from a given layer. The findings from XPS provide an insightful explanation for the decrease in saturation magnetization (Ms) observed with the increase in annealing temperature to 1073 K. Interdiffusion occurring between the NdFe and tantalum (Ta) layers at high temperatures induces modifications in the films' structure and composition, exerting a direct influence on their magnetic properties. These discoveries provide new insights into the fundamental mechanisms governing the transformations in

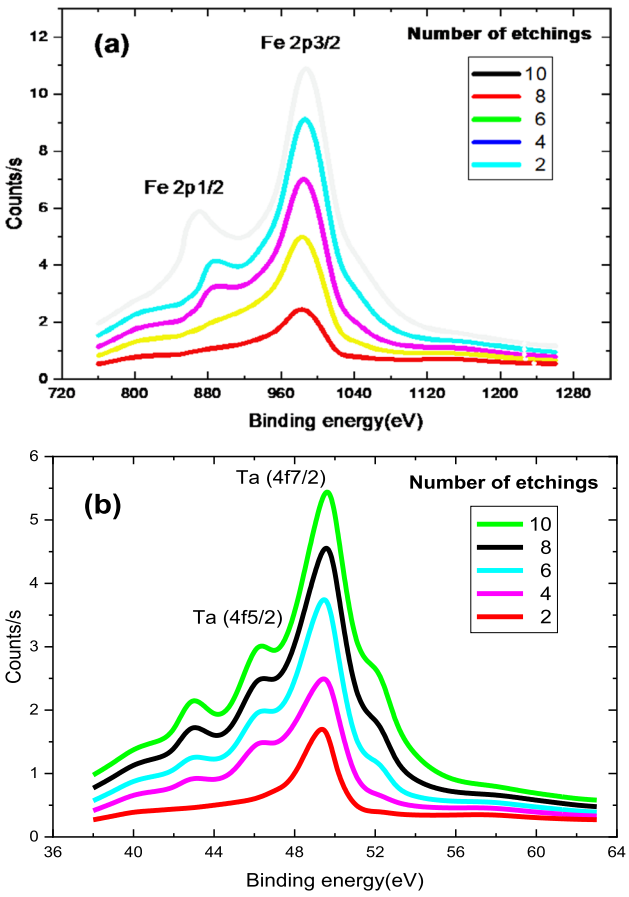

Fig. 13 XPS depth profiles of **a** the Fe 2p1/2 and Fe 2p3/2, **b** the Ta 4f5/2 and Ta 4f7/2 for NdFe/MgO (001) films as a function of etching number

the magnetic behavior within the NdFe/MgO (001) films in response to high annealing temperatures.

The results obtained in this study have highlighted the effectiveness of several parameters in enhancing the efficiency of the reactions. Firstly, the use of a direct current magnetron sputtering system under ultra-high vacuum conditions allowed precise control over the composition and structure of the films. This precision is crucial because the magnetic properties of the films closely depend on their composition and structure. Furthermore, employing a nanocrystalline Nd3Fe29 alloy target facilitated the creation of films with a more uniform grain size. Uniform grain size is of paramount importance for the magnetic properties of the films as it reduces defects and impurities. Finally, the use of a variable-temperature annealing process improved the crystallinity and microstructure of the films. This improvement resulted in a notable increase in coercivity (Hc), magnetic remanence (Mr), and magnetic anisotropy (Ha) of the films.

4 Conclusion

This study conducts a thorough analysis of NdFe/MgO (001) films, exploring their structural and magnetic properties under various thicknesses and heat treatments. Using techniques like X-ray diffraction, SEM, MFM, and FMR, the research delves into the intricate relationship between film structure, grain size, and magnetic behavior. Remarkable results were observed in a 250 nm NdFe/MgO (001) film annealed at 873 K, showcasing robust magnetic properties. The study reveals correlations between key magnetic traits, grain size, domain arrangement, and thermal treatments, highlighting a complex evolution with increasing film thickness. Additionally, XPS analyses uncover interdiffusion phenomena, influencing magnetic properties. While providing valuable insights, the study leaves gaps in understanding property interconnections, necessitating future research through simulations and theoretical modeling.

Author contributions RF: Conceptualization, methodology, structure and microstructure characterization, data curation, formal analysis, writing—original draft. APD: Methodology, magnetic characterization, investigation, data curation, writing—review and editing.

Data availability The data that support the findings of this study are available from the corresponding author upon reasonable request. This work has never been published before.

Declarations

Conflict of interest The authors declare that they have no known competing financial interests or personal relationships that could have appeared to influence the work reported in this paper.

References

1. C. Heck, *Magnetic materials and their applications* (Elsevier, 1974)
2. P. Campbell, *Permanent magnet materials and their application* (Cambridge University Press, 1994)
3. F. P. Missell (eds), "Magnetism, Magnetic Materials and Their Applications," CD-ROM, January 20, (1999)
4. M. Amiri, K. Eskandari, M.S. Niasari, Adv. Colloid Interface Sci. **271**, 101982 (2019)
5. C.-J. Yang, W.-Y. Lee, S.-D. Choi, J. Magn. Magn. Mater. **114**, 18 (1992)
6. G. Schneider, F.J.G. Landgraf, V. Villas-Boas, G.H. Bezerra, F.P. Missell, A.E. Ray, Mater. Lett. **8**, 472 (1989)
7. Z. Heydariyan, R. Monsef, M.S. Niasari, J. Alloys Compd. **924**, 166564 (2022)
8. G. Florio, Applications of magnetic material, in *Encyclopedia of smart materials*, vol. 5, (Elsevier, 2022), p.24
9. A. Nakhlband, H.K. Kordasht, M. Rahimi, A. Mokhtarzadeh, J. Soleymani, Microchem. J. **173**, 107042 (2022)
10. I. Stoica, A. R. Abraham, A. K. Haghi (eds.), "Modern Magnetic Materials: Properties and Applications," December 2023, Hardback ISBN: 9781774912997, E-Book ISBN: 9781003372066.
11. R.C. Taylor et al., J. Appl. Phys. **49**, 2886 (1978)
12. T. Suzuki, J. Magn. Magn. Mater. **50**, 265 (1985)
13. P. Guo-hong, W. Qin-tang, G. Qing-chun, J. Magn. Magn. Mater. **104–107**, 981 (1992)
14. D. Dai et al., J. Appl. Phys. **57**, 3589 (1985)
15. R. Carey et al., J. Magn. Magn. Mater. **50**, 335 (1985)
16. P.G. Hong, W.Q. Tang, G.Q. Chun, J. Magn. Magn. Mater. **104–107**, 981 (1992)
17. M.R. Jian, T.S. Chin, J.L. Tsai, H.W. Zhang, B.G. Shen, J. Magn. Magn. Mater. **209**, 205 (2000)
18. J.L. Schroeder, A.S. Ingason, J. Rosén, J. Birch, J. Crystal Growth **420**, 22 (2015)
19. S. Chikazumi, *Physics of ferromagnetism*, 2nd edn. (Oxford University Press, 2009)
20. V. Komogortsev, T.N. Patrusheva, D.A. Balaev, E.A. Denisova, I.V. Ponomarenko, Tech. Phys. Lett. **35**, 882 (2009)
21. R. Monsef, M.G. Arani, M.S. Niasari, Ultrason. Sonochem. **42**, 201 (2018)
22. R. Fersi, N. Mliki, L. Bessais, R. Guetari, V. Russier, M. Cabié, J. Alloys Compd. **522**, 14 (2012)
23. K. Dubey, S. Dubey, V. Sahu, R.A. Parry, A. Modi, N.K. Gaur, Appl. Phys. A **128**, 560 (2022)
24. C. Chappert, K. Le Dang, P. Beauvillain, H. Hurdequint, D. Renard, Phys. Rev. B **34**, 3192 (1986)
25. P. Liu, V.M. Hong Ng, Z. Yao, J. Zhou, Y. Lei, Z. Yang, H. Lv, L.B. Kong, ACS Appl. Mater. Interfaces **9**, 16404 (2017)
26. P. Liu, Z. Yao, J. Zhou, Z. Yang, L.B. Kong, J. Mater. Chem. C **4**, 9738 (2016)

27. M. Amiri, M.S. Niasari, A. Akbari, T. Gholami, Int. J. Hydrog. Energy **42**(39), 24846 (2017)
28. A.P. Dalia, R. Fersi, J. Magn. Magn. Mater. **532**, 167874 (2021)
29. R. Fersi, A.P. Dalia, J. Appl. Phys. **128**(6), 540 (2022)
30. R. Fersi, A.P. Dalia, J. Supercond. Nov. Magn. **35**(10), 2923 (2022)
31. A. Walther, C. Marcoux, B. Desloges, R. Grechishkin, D. Givord, N.M. Dempsey, J. Magn. Magn. Mater. **321**(6), 590 (2009)
32. Y. Gong, Z. Qiu, S. Liang, X. Zheng, H. Meng, Z. Zheng, D. Chen, S. Yuan, W. Xia, D. Zeng, J.P. Liu, J. Rare Earths (2023). https://doi.org/10.1016/j.jre.2023.06.012. (**ISSN 1002-0721**)
33. M.S. Niasari, D. Ghanbari, F. Davar, J. Alloys Compd. **492**, 570 (2010)
34. M.S. Niasari, M. Dadkhah, F. Davar, Polyhedron **28**(14), 3005 (2009)